

# Orbital dependent electron tunneling within the atom superposition approach: Theory and application to W(110)

Krisztián Palotás\* and Gábor Mándi

*Budapest University of Technology and Economics,  
Department of Theoretical Physics, Budafoki út 8., H-1111 Budapest, Hungary*

László Szunyogh

*Budapest University of Technology and Economics,  
Department of Theoretical Physics and Condensed Matter  
Research Group of the Hungarian Academy of Sciences,  
Budafoki út 8., H-1111 Budapest, Hungary*

(Dated: June 29, 2012)

## Abstract

We introduce an orbital dependent electron tunneling model and implement it within the atom superposition approach for simulating scanning tunneling microscopy (STM) and spectroscopy (STS). Applying our computationally efficient method, we analyze the convergence and the orbital contributions to the tunneling current and the corrugation of constant current STM images above the W(110) surface. In accordance with a previous study, we find corrugation reversals depending on the bias voltage and the tip-sample distance. Explaining this effect, we highlight the role of the real space shape of the orbitals involved in the tunneling. Moreover, we calculate corrugation inversion maps considering different tip models, and find two qualitatively different behaviors based on the tip orbital symmetry. From these maps, we predict corrugation reversals for specific tips even at positive bias voltages at enlarged tip-sample distances compared to those at negative bias.

PACS numbers: 68.37.Ef, 71.15.-m, 73.63.-b

---

\*Electronic address: palotas@phy.bme.hu

## I. INTRODUCTION

The experimental use of scanning tunneling microscopy (STM) and spectroscopy (STS) has recently gained a boost, particularly for studying magnetic systems [1–3]. The experimentally observed effects are not straightforward to explain without a proper theoretical support [4, 5]. One direction of recent theoretical research is focused on extracting surface local electronic properties from experimental STS data [6–10], which is the convolution of tip and sample electronic structures. Another research direction is concerned with the simulation of STM and STS by using different models, mostly based on electronic structure data obtained from first principles. Some recently developed approaches highlight the importance of the inclusion of the tip electronic structure into the tunneling model [8, 11, 12], and it is also possible to separate tip and sample contributions to STS [13].

The atom superposition approach for simulating STM [14] and STS [15] is a computationally efficient method. In the present work we go beyond the so-called independent orbital approximation and consider a simple model for orbital dependent tunneling. The reliability of this new method is demonstrated by the analysis of the tip-sample distance and bias voltage dependent corrugation reversal effect observed on the W(110) surface, where we find excellent agreement with a previous work [16] at much lower computational costs. The computational efficiency of our method enables us to study this effect in more detail. We particularly focus on tip effects, and consider ideal tip models with different orbital symmetries, and a more realistic W(110) tip. We find two qualitatively different corrugation inversion behaviors based on the tip orbital symmetry. Moreover, we predict corrugation reversals for specific tips even at positive bias voltages at enlarged tip-sample distances compared to those at negative bias.

The paper is organized as follows: The theoretical model of the orbital dependent tunneling within the atom superposition approach is presented in section II. Applying this method, we investigate the convergence and the orbital contributions of the tunneling current, as well as the corrugation reversal of the W(110) surface depending on the applied bias voltage and the tip-sample distance in section III. Summary of our findings is found in section IV.

## II. THEORETICAL MODEL OF ORBITAL DEPENDENT TUNNELING

Recently, Palotás et al. developed a three-dimensional (3D) atom superposition approach for simulating spin-polarized STM (SP-STM) [14] and spin-polarized STS (SP-STs) [15] based on previous theories [8, 17–20]. The main advance was the inclusion of the tip electronic structure, thus, tip dependent tunneling properties can be studied. In the model, it is assumed that electrons tunnel through one tip apex atom, and contributions from individual transitions between this apex atom and each of the surface atoms are summed up assuming the one-dimensional (1D) Wentzel-Kramers-Brillouin (WKB) approximation for electron tunneling processes in all these transitions. The key input is the projected electron density of states (PDOS) of the tip apex atom and of the sample surface atoms obtained from ab initio electronic structure calculations. In the present paper, first, we review the tunneling current and the differential conductance expressions based on the independent orbital approximation for the vacuum decay of electron states, and then we extend this model to include a simple orbital dependent tunneling transmission. We consider the non-spin-polarized part of the tunneling only, however, this theory can be applied to SP-STM and SP-STs in the future.

Assuming  $T = 0$  K temperature, the tunneling current at the tip position  $\underline{R}_{TIP}(x, y, z)$  and at bias voltage  $V$  is given by

$$I(x, y, z, V) = \int_0^V \frac{dI}{dU}(x, y, z, U, V) dU. \quad (1)$$

The integrand is the so-called virtual differential conductance,

$$\begin{aligned} \frac{dI}{dU}(x, y, z, U, V) &= \varepsilon^2 \frac{e^2}{h} \\ &\times \sum_a T(E_F^S + eU, V, d_a(x, y, z)) n_T(E_F^T + eU - eV) n_S^a(E_F^S + eU). \end{aligned} \quad (2)$$

Here,  $e$  is the elementary charge,  $h$  is the Planck constant, and  $E_F^T$  and  $E_F^S$  are the Fermi energies of the tip and the sample surface, respectively.  $\varepsilon^2 e^2/h$  ensures that the  $dI/dU$  is correctly measured in the units of  $A/V$ .  $\varepsilon$  has been chosen to 1 eV, but its actual value has to be determined comparing simulation results to experiments. The sum over  $a$  corresponds to the atomic superposition and has to be carried out, in principle, over all surface atoms. Convergence tests, however, showed that including a relatively small number of atoms in the sum provides converged  $dI/dU$  values [12].  $T(E_F^S + eU, V, d_a(x, y, z))$  is the energy

and bias dependent tunneling transmission function, which also depends on the distance  $d_a(x, y, z) = |\underline{R}_{TIP}(x, y, z) - \underline{R}_a|$  between the tip apex and the surface atom labeled by  $a$  with position vector  $\underline{R}_a$ . The tip and sample electronic structures are included into this model via projected DOS (PDOS) onto the atoms, i.e.,  $n_T(E)$  and  $n_S^a(E)$  denote projected charge DOS onto the tip apex and the  $a$ th surface atom, respectively. They can be obtained from any suitable electronic structure method.

Taking the derivative of Eq.(1) with respect to the bias voltage, the differential conductance is obtained. It can be written at the tip position  $\underline{R}_{TIP}(x, y, z)$  and at bias voltage  $V$  as the sum of three terms,

$$\frac{dI}{dV}(x, y, z, V) = \frac{dI}{dU}(x, y, z, V, V) + B(x, y, z, V) + D_T(x, y, z, V). \quad (3)$$

Here,  $dI/dU$  has been defined in Eq.(2), and  $B$  and  $D_T$  are the background and tip-derivative terms,

$$B(x, y, z, V) = \varepsilon^2 \frac{e^2}{h} \quad (4)$$

$$\times \sum_a \int_0^V \frac{\partial T}{\partial V}(E_F^S + eU, V, d_a(x, y, z)) n_T(E_F^T + eU - eV) n_S^a(E_F^S + eU) dU,$$

$$D_T(x, y, z, V) = -\varepsilon^2 \frac{e^2}{h} \quad (5)$$

$$\times \sum_a \int_0^V T(E_F^S + eU, V, d_a(x, y, z)) \frac{\partial n_T}{\partial U}(E_F^T + eU - eV) n_S^a(E_F^S + eU) dU,$$

respectively [15]. The background term, which contains the bias-derivative of the transmission function, is usually taken into account in recent STS theories [8, 21, 22], while the tip-derivative term containing the energy derivative of the tip DOS is rarely considered in the recent literature.

In the spirit of the independent orbital approximation, the transmission probability for electrons tunneling between states of atom  $a$  on the surface and the tip apex is of the simple form,

$$T(E_F^S + eU, V, d_a) = e^{-2\kappa(U, V)d_a}. \quad (6)$$

This corresponds to a spherical exponential decay of the electron wave functions irrespective of their orbital symmetry [20, 23, 24]. Assuming the same effective rectangular potential barrier between the tip apex and each surface atom, the vacuum decay  $\kappa$  can be written as

$$\kappa(U, V) = \frac{1}{\hbar} \sqrt{2m \left( \frac{\phi_S + \phi_T + eV}{2} - eU \right)}, \quad (7)$$

where the electron's mass is  $m$ ,  $\hbar$  is the reduced Planck constant, and  $\phi_S$  and  $\phi_T$  are the average electron work function of the sample surface and the local electron work function of the tip apex, respectively. The method of determining the electron work functions from the calculated local electrostatic potential is reported in Ref. [14].

Next, we extend this tunneling model by taking advantage of the orbital decomposition of the electronic structure data and the real space shape of the electron orbitals. The PDOS of the sample surface atoms and the tip apex can be decomposed according to orbital symmetry, i.e., real spherical harmonics,  $\beta, \gamma \in \{s, p_y, p_z, p_x, d_{xy}, d_{yz}, d_{3z^2-r^2}, d_{xz}, d_{x^2-y^2}\}$ , as

$$n_S^a(E) = \sum_{\beta} n_{S\beta}^a(E), \quad (8)$$

$$n_T(E) = \sum_{\gamma} n_{T\gamma}(E). \quad (9)$$

Assuming such an orbital decomposition, the virtual differential conductance can be generalized as

$$\begin{aligned} \frac{dI}{dU}(x, y, z, U, V) &= \varepsilon^2 \frac{e^2}{h} \\ &\times \sum_a \sum_{\beta, \gamma} T_{\beta\gamma}(E_F^S + eU, V, d_a(x, y, z)) n_{T\gamma}(E_F^T + eU - eV) n_{S\beta}^a(E_F^S + eU), \end{aligned} \quad (10)$$

where, additionally to the atomic superposition (sum over  $a$ ), we sum up each  $\beta \leftrightarrow \gamma$  transition with an orbital dependent tunneling transmission:  $T_{\beta\gamma}(E, V, d_a)$  gives the electron tunneling probability at energy  $E$  from the tip apex  $\gamma$  orbital to the  $\beta$  orbital of the  $a$ th surface atom at positive bias voltage ( $V > 0$ ), and from the  $\beta$  orbital of the  $a$ th surface atom to the tip apex  $\gamma$  orbital at negative bias ( $V < 0$ ).  $T_{\beta\gamma}$  can be defined in different ways based on physical arguments. We consider the following form,

$$T_{\beta\gamma}(E_F^S + eU, V, d_a) = e^{-2\kappa(U, V)d_a} t_{\beta\gamma}(\vartheta_a, \varphi_a) \quad (11)$$

for each surface atom  $\leftrightarrow$  tip apex 1D electron transition. Here, the energy and bias dependent part corresponds to the spherical exponential decay considered in Eq.(6), and is independent of the orbital symmetry. This is multiplied by an orbital dependent expression  $t_{\beta\gamma}$ , which depends on the spatial arrangement of the sample atoms relative to the tip apex and all the orbital shapes involved in the tunneling. The angular dependence on  $\vartheta_a$  and  $\varphi_a$  comes into play in the following way: Let us consider one transition between surface atom  $a$  and the tip apex along the line connecting the two atoms. A particular geometry is shown in

Figure 1. For brevity, we omitted the  $a$  notation of the surface atom. For both atoms, a local coordinate system can be set up, and the angular dependence of the atomic orbital wave functions,  $\chi(\vartheta, \varphi)$ , are defined in the corresponding coordinate system, as summarized in Table I.  $\underline{R}_{TIP} - \underline{R}_a$  defines a vector pointing from the surface atom toward the tip apex, and it can be represented by the  $(d_a, \vartheta_a, \varphi_a)$  coordinates in the spherical coordinate system centered on the  $a$ th surface atom. Taking the opposite connecting vector from the tip apex toward the surface atom, its coordinates are  $(d_a, \pi - \vartheta_a, \pi + \varphi_a)$  in the spherical coordinate system centered on the tip apex. According to Figure 1,  $d_a$ ,  $\vartheta_a$ , and  $\varphi_a$  can be calculated as

$$d_a = \sqrt{(x - x_a)^2 + (y - y_a)^2 + (z - z_a)^2}, \quad (12)$$

$$\vartheta_a = \arccos \left( \frac{z - z_a}{d_a} \right), \quad (13)$$

$$\varphi_a = \arccos \left( \frac{x - x_a}{d_a \sin(\vartheta_a)} \right), \quad (14)$$

using the global coordinates  $\underline{R}_{TIP} = (x, y, z)$  and  $\underline{R}_a = (x_a, y_a, z_a)$ . Considering above,  $t_{\beta\gamma}$  accounts for the modification of the perfect spherical exponential decay along the connecting line through the angular dependence of the atomic orbitals as

$$t_{\beta\gamma}(\vartheta_a, \varphi_a) = [\chi_\beta(\vartheta_a, \varphi_a)]^2 \times [\chi_\gamma(\pi - \vartheta_a, \pi + \varphi_a)]^2, \quad (15)$$

where  $\chi_{\beta,\gamma}(\vartheta, \varphi)$  are the real spherical harmonics summarized in Table I. They were chosen in such a way that  $0 \leq t_{\beta\gamma} \leq 1$ . This factor takes the effect of the directional tunneling between real space orbitals into account. The physical motivation is the angular dependence of the electron density of the orbitals in the given tunneling direction, which modifies the tunneling transmission. The maximum  $t = 1$  is obtained if the angular distributions of the electron density according to the given orbital symmetries  $(\beta, \gamma)$  around both the sample surface atom and the tip apex have maxima along the line of the tunneling direction. This is always the case for  $s$ - $s$  type of tunneling irrespective of the relative position of the tip apex and sample surface atoms, i.e., we observe perfect spherical exponential decay between tip and sample  $s$  orbitals. In some particular geometries  $t = 1$  can be obtained even for other type of orbitals, e.g., if the tip apex is precisely above surface atom  $a$ , i.e.,  $\vartheta_a = 0$ , then  $t_{\beta\gamma}(\vartheta_a = 0, \varphi_a) = 1$  for all of the following combinations:  $\beta, \gamma \in \{s, p_z, d_{3z^2-r^2}\}$ . On the other hand, if the tip apex is above surface atom  $a$ , then orbitals with nodal planes orthogonal to the surface have zero contribution to the tunneling from this particular surface atom, i.e., a reduced effective

tunneling transmission is obtained [25]. Note that the independent orbital approximation corresponds to  $t_{\beta\gamma} = 1$  for all  $\beta \leftrightarrow \gamma$  transitions, i.e., the same tunneling transmission is assumed between all orbitals. Within our orbital dependent tunneling approach, ideal tip models with particular orbital symmetries can be considered, i.e.,  $\gamma_0$  orbital symmetry corresponds to the choice of  $n_{T\gamma_0} = 1(eV)^{-1}$  and  $n_{T(\gamma \neq \gamma_0)} = 0$ . More realistic tips can be obtained by explicitly calculating the orbital decomposition of the tip apex PDOS in model tip geometries, e.g., in the present work a model W(110) tip is used.

Our theory is, thus, an extension of the atom superposition STM/STS approach considering tunneling between directional orbitals. The tunneling current and the differential conductance can be calculated at the tip position  $\underline{R}_{TIP}(x, y, z)$  and at bias voltage  $V$  as the sum of all  $\beta \leftrightarrow \gamma$  transitions between real space orbitals,

$$I(x, y, z, V) = \sum_{\beta, \gamma} I_{\beta\gamma}(x, y, z, V), \quad (16)$$

$$\frac{dI}{dV}(x, y, z, V) = \sum_{\beta, \gamma} \frac{dI_{\beta\gamma}}{dV}(x, y, z, V), \quad (17)$$

respectively, with

$$I_{\beta\gamma}(x, y, z, V) = \varepsilon^2 \frac{e^2}{h} \quad (18)$$

$$\begin{aligned} & \times \sum_a \int_0^V T_{\beta\gamma}(E_F^S + eU, V, d_a(x, y, z)) n_{T\gamma}(E_F^T + eU - eV) n_{S\beta}^a(E_F^S + eU) dU, \\ & \frac{dI_{\beta\gamma}}{dV}(x, y, z, V) = \varepsilon^2 \frac{e^2}{h} \quad (19) \\ & \times \left\{ \sum_a T_{\beta\gamma}(E_F^S + eV, V, d_a(x, y, z)) n_{T\gamma}(E_F^T) n_{S\beta}^a(E_F^S + eV) \right. \\ & + \sum_a \int_0^V \frac{\partial T_{\beta\gamma}}{\partial V}(E_F^S + eU, V, d_a(x, y, z)) n_{T\gamma}(E_F^T + eU - eV) n_{S\beta}^a(E_F^S + eU) dU \\ & \left. - \sum_a \int_0^V T_{\beta\gamma}(E_F^S + eU, V, d_a(x, y, z)) \frac{\partial n_{T\gamma}}{\partial U}(E_F^T + eU - eV) n_{S\beta}^a(E_F^S + eU) dU \right\}. \end{aligned}$$

This decomposition enables the analysis of the orbital contributions to the total tunneling current and to the differential conductance. In relation to Chen's derivative rule [26], we can state that while it is formulated inspired by the Tersoff-Hamann model, and calculates the tunneling transmission as the absolute value square of the tunneling matrix element, that is proportional to the sample wave function derivative with respect to the real space

coordinate corresponding to the given tip orbital symmetry ( $\gamma$ ), our transmission function also depends on the sample surface atoms' orbital symmetry  $\beta$ . Moreover, in our theory the electronic structure of the tip apex via the PDOS is accounted for. Note that the presented method can also be applied to magnetic systems taking into account the orbital-decomposed magnetization PDOS of the tip and sample [14, 15] together with the orbital dependent tunneling transmission in Eq.(11). As it was pointed out by Ferriani et al. [27], the spin polarization in the vacuum can have an opposite sign than within the tip apex atom, and this sign change is also accompanied by different dominating orbital characters. Thus, the consideration of an orbital dependent tunneling transmission might be a better model for describing electron transport through a magnetic tunnel junction. We return to the related spin-polarized STM/STS model in the future.

### III. RESULTS AND DISCUSSION

In order to demonstrate the reliability of our orbital dependent tunneling model we consider a W(110) surface. This surface has technological importance as it is widely used as substrate for thin film growth, see e.g., Refs. [16, 28]. As it was pointed out by Heinze et al. [16], the determination of the position of surface atomic sites is not straightforward, as atomic resolution is lost at negative bias voltages, and a bias-dependent corrugation reversal has been predicted. This means that normal and anticorrugated constant current STM images can be obtained in certain bias voltage ranges, and the W atoms do not always appear as protrusions in the images. It was shown that a competition between states from different parts of the surface Brillouin zone is responsible for this effect [16, 29]. We reinvestigate this corrugation reversal effect, as it provides a challenge for our orbital dependent tunneling model. We find excellent agreement with the results of Ref. [16], where an *s*-wave tip has been used, and since our method is computationally more efficient, we study this effect in more detail. We particularly focus on tip effects, and consider ideal tip models with different orbital symmetries, and a more realistic W(110) tip. We find two qualitatively different corrugation inversion behaviors based on the tip orbital symmetry. Moreover, we predict corrugation reversals for specific tips even at positive bias voltages at enlarged tip-sample distances compared to those at negative bias. Explaining our findings, we highlight the role of real space orbital orientational overlaps between the surface and the tip rather than



considering electron states in the reciprocal space, thus, a different kind of understanding is provided.

We performed geometry relaxation and electronic structure calculations based on the density functional theory (DFT) within the generalized gradient approximation (GGA) implemented in the Vienna Ab-initio Simulation Package (VASP) [30–32]. A plane wave basis set for electronic wave function expansion together with the projector augmented wave (PAW) method [33] has been applied, and the exchange-correlation functional is parametrized according to Perdew and Wang (PW91) [34].

We model the W(110) surface by a slab of nine layers, where the two topmost W layers have been fully relaxed. After relaxation the W-W interlayer distance between the two topmost layers is reduced by 3.3%, while the underneath W-W interlayer distance increased by 1.1% compared to bulk W. A separating vacuum region of 18 Å width in the surface normal ( $z$ ) direction has been set up between neighboring supercell slabs. The average electron work function above the surface is calculated to be  $\phi_S = 4.8$  eV. We used a  $15 \times 15 \times 3$  Monkhorst-Pack (MP) [35] k-point grid for calculating the orbital-decomposed projected electron DOS,  $n_{S\beta}^a(E)$ , onto the surface W atom. The unit cell of the W(110) surface (shaded area) and the rectangular scan area for the tunneling current simulation are shown in Figure 2. In our calculations we used the experimental lattice constant  $a = 316.52$  pm. Moreover, the surface top (T) and hollow (H) positions are explicitly shown.

We considered different tip models. The orbital-independent ideal tip is characterized by  $t_{\beta\gamma} = 1$  and  $n_{T\gamma}(E) = 1/9(eV)^{-1}$ , so that  $n_T(E) = \sum_{\gamma} n_{T\gamma}(E) = 1(eV)^{-1}$ . This ideal electronically flat tip represents the limiting case of the independent orbital approximation used in previous atom superposition tunneling models [12, 14, 15, 20]. In order to study the effect of the orbital dependent tunneling, other tip models are needed. First, we consider ideal tip models having a particular orbital symmetry  $\gamma_0$ . In this case,  $t_{\beta\gamma}$  is calculated following Eq.(15), and for the energy dependence of the tip PDOS,  $n_{T\gamma_0} = 1(eV)^{-1}$  and  $n_{T(\gamma \neq \gamma_0)} = 0$  are assumed. More realistic tips can also be employed by calculating the orbital decomposition of the tip apex PDOS in model tip geometries, and using Eq.(15) for the orbital dependent transmission factor. We used a W(110) tip. It has been modeled by a slab consisting of seven atomic layers, having one W apex atom on both surfaces, i.e., with a double vacuum boundary. In this system the apex atom and the topmost surface layers have been relaxed on both sides. The interlayer distance between the topmost W

layer and the underneath one was reduced by 0.9%, while the adatom-topmost layer vertical distance decreased by 21.2% compared to bulk W. The interaction between apex atoms in neighboring supercells in the lateral direction is minimized by choosing a  $3 \times 3$  surface cell, and a 16.7 Å wide separating vacuum region in the  $z$  direction. Moreover, an  $11 \times 11 \times 1$  MP k-point grid has been chosen for obtaining the orbital-decomposed projected DOS,  $n_{T\gamma}(E)$ , onto the apex atom. The local electron work function above the tip apex is  $\phi_T = 4.36$  eV.

Previously, the convergence of the  $dI/dU$  part of the differential conductance has been investigated with respect to the number of surface atoms involved in the summation of the orbital-independent atomic superposition formula [12]. Due to the spherical exponential decay assumed for the electron wave functions, a rapid convergence was found. We report a similar convergence test for the orbital-dependent tunneling approach, comparing different tip models. In order to take into account a wide energy range around the Fermi level, we calculated the tunneling current at -2.5 V and +2.5 V bias voltages at  $z = 4.5$  Å above a surface W atom, and averaged these current values. We considered ideal tips of the orbital-independent model, and with  $s$ ,  $p_z$ , and  $d_{3z^2-r^2}$  symmetry, as well as the W(110) tip. In order to obtain comparable results, we normalized the averaged current for each tip calculation. The convergences of the normalized averaged current with respect to the lateral distance on the surface,  $d_{\parallel}$ , characteristic for the number of atoms involved in the atomic superposition, are shown in Figure 3. By calculating the current, contributions from surface atoms within a radius of  $d_{\parallel}$  measured from the W atom below the tip apex are summed up (sum over  $a$ ). We find that the orbital-independent, the  $s$ -type, and the W(110) tips behave quite similarly concerning the current convergence, while for the  $p_z$ - and  $d_{3z^2-r^2}$ -type tips a faster convergence is found. This rapid convergence can be explained by the more localized character of the latter tip orbitals in the direction normal to the sample surface ( $z$ ). On the other hand, the orbital-independent tip with  $T = e^{-2\kappa d}$  is a good approximation for the  $s$ -type tip (with index  $\gamma = 1$ ), where the spherically decaying transmission function part is still dominant, i.e.,  $T_{\beta,1} = e^{-2\kappa d} \chi_{\beta}^2$  because  $\chi_1^2 = 1$ . In case of the W(110) tip, electronic states of all considered symmetries have a contribution, and their relative importance is not only determined by the transmission function via the orbital shapes, but also by the product of the symmetry-decomposed electron PDOS of the surface and the tip. In general, the orbitals localized in different than the  $z$  direction can show a slower current convergence than the  $s$  orbitals. However, the partial PDOS of such states is relatively low, and, interestingly,

we obtain a similar current convergence in the studied energy range as for the  $s$ -type tip. Choosing different bias voltages, and, thus, different electron states involved in the tunneling, for the W(110) tip we found current convergences dissimilar to the  $s$ -type tip behavior. The convergence can be slower or faster than obtained for the  $s$ -type tip, depending on the partial PDOS of each directional orbitals in the given energy range.

Based on the convergence tests, atom contributions from at least  $d_{\parallel} = 3a \approx 9.5 \text{ \AA}$  distance from the surface-projected tip position shall be considered. In case of calculating STM images,  $d_{\parallel} = 3a \approx 9.5 \text{ \AA}$  has to be measured from the edge of the scan area in all directions in order to avoid distortion of the image, thus, involving 67 surface atoms in the atomic superposition. For brevity, in the following, we use the same surface atoms to calculate single point tunneling properties as well.

Let us analyze the relative importance of all  $\beta \leftrightarrow \gamma$  transitions in determining the total tunneling current at different tip positions. From this analysis we obtain a qualitative picture about the role of the different atomic orbitals in the construction of the tunneling current. The  $I_{\beta\gamma}$  current contributions can be calculated according to Eq.(18). These can be represented by a current histogram, that gives the percentual contributions of the individual transitions to the total current. Figure 4 shows such histograms using the W(110) tip at  $V = -0.1 \text{ V}$  bias voltage,  $z = 4.5 \text{ \AA}$  above two different tip positions: part a) corresponds to the tip apex above the surface top position, and part b) to the tip apex above the surface hollow position, T and H in Figure 2, respectively. We obtain a  $9 \times 9$  matrix from the considered orbitals, which are denoted by numbers 1 to 9 following the indices reported in Table I. We find that most contributions are due to the  $s$  (1),  $p_z$  (3),  $d_{yz}$  (6),  $d_{3z^2-r^2}$  (7), and  $d_{xz}$  (8) orbitals and their combinations. The largest contribution to the current is given by the  $d_{3z^2-r^2} - d_{3z^2-r^2}$  (7-7) transition in both considered tip positions. While it corresponds to 25 per cent above the top position, it is slightly lower, 18 per cent above the hollow position. Concomitantly, above the hollow position, the relative importance of both tip and sample  $d_{yz}$  (6) and  $d_{xz}$  (8) orbitals is increased as it is expected from the geometrical setup, i.e., the  $d_{yz} - d_{yz}$  (6-6),  $d_{yz} - d_{3z^2-r^2}$  (6-7 and 7-6),  $d_{xz} - d_{xz}$  (8-8), and  $d_{xz} - d_{3z^2-r^2}$  (7-8 and 8-7) contributions correspond to larger orientational overlap of the mentioned tip and sample orbitals if the tip is above the hollow position rather than above the top position, as suggested by Fig. 2 and Eq.(15). Thus, our simple orbital dependent tunneling model captures the effect of the localized orbitals and goes beyond the spherical

Tersoff-Hamann model. Note that if a larger bias voltage is considered, i.e., the electronic states are somewhat averaged, then the independent orbital approach might turn out to be a good approximation [20].

The role of the localized orbitals can best be demonstrated by returning to the corrugation inversion phenomenon found, e.g., on (110) transition metal surfaces [16]. Under certain circumstances the apparent height of W atoms at the surface top position ( $z_T$ ) can be larger or smaller than the apparent height of the surface hollow position ( $z_H$ ) at constant current ( $I = \text{const}$ ) condition. (For the surface top (T) and hollow (H) positions, see Figure 2.) Thus, the sign change of  $\Delta z(I) = z_T(I) - z_H(I)$  is indicative for the corrugation inversion. Obviously,  $\Delta z(I) > 0$  corresponds to a normal STM image, where the W atoms appear as protrusions, and  $\Delta z(I) < 0$  to an anticorrugated image. Since the tunneling current is monotonously decreasing with the increasing tip-sample distance, we can obtain information about the occurrence of the corrugation inversion simply by calculating the current difference between tip positions above the top and hollow sites of the W(110) surface. The current difference at tip-sample distance  $z$  and at bias voltage  $V$  is defined as

$$\Delta I(z, V) = I_T(z, V) - I_H(z, V). \quad (20)$$

This quantity can be calculated for specific tips, and we call the  $\Delta I(z, V) = 0$  contour as the corrugation inversion map. This gives the  $(z, V)$  combinations where the corrugation inversion occurs. The sign of  $\Delta I(z, V)$  provides the corrugation character of an STM image in the given  $(z, V)$  regime. Due to the monotonously decreasing character of the tunneling current,  $\Delta I(z, V) > 0$  corresponds to  $\Delta z(I(V)) > 0$ , i.e., normal corrugation, and the same holds for the opposite relation, i.e.,  $\Delta I(z, V) < 0$  corresponds to  $\Delta z(I(V)) < 0$  and anticorrugation.

First, we calculated  $\Delta I(z, V)$  using the independent orbital approximation and Eq.(6) for the tunneling transmission, and found that  $\Delta I(z, V)$  is always positive. This means that the spherical exponential decay itself can not account for the observed corrugation inversion effect, and the W atoms always appear as protrusions in STM images calculated with this model. However, considering the orbital dependent tunneling transmission, Eq.(11), we find evidence for the corrugation inversion effect, thus, highlighting the role of the real space shape of electron orbitals involved in the tunneling. Figure 5 shows  $\Delta I(z, V) = 0$  contours calculated with different tip models in the  $[0 \text{ \AA}, 14 \text{ \AA}]$  tip-sample distance and  $[-2 \text{ V}, +2 \text{ V}]$

bias voltage range. Before turning to the analysis of the results obtained with previously not considered tip models, let us compare our results with those of Heinze et al. [16], where an  $s$ -wave tip model has been used. They found corrugation reversal at around  $-0.4$  V at  $z = 4.6$  Å tip-sample distance, and above that voltage normal, while below that anticorrugated STM images were obtained. Our model with an  $s$ -tip provides the same type of corrugation reversal at  $-0.23$  V at the same distance as can be seen in part b) of Figure 5 (curve with square symbol). These values are in reasonable agreement, particularly concerning their negative bias value, where atomic resolution is difficult to achieve experimentally, which is an indication for being close to the corrugation inversion regime [16]. On the other hand, a linear dependence of the corrugation reversal voltage and the tip-sample distance has been reported by Heinze et al. ( $z = 4.6$  Å,  $V = -0.4$  V) to ( $z = 7.2$  Å,  $V = 0$  V). Our model qualitatively reproduces this linear dependence in the same bias range, though the quantitative values are somewhat different.

Calculating the corrugation inversion maps with more tip models, we find two distinct behaviors depending on the tip orbital symmetry. Parts a) and b) of Figure 5 show these. While, there is no corrugation inversion occurring at positive bias voltages for tip models in part a), tips in part b) show this effect also at positive bias. Moreover, in both parts anticorrugation is observed in the large tip-sample distance region ( $z > 13.5$  Å) as  $\Delta I(z, V) < 0$  there. This is in accordance with the prediction of Ref. [29] based on the analysis of the competing electron states in the surface Brillouin zone for an Fe(001) surface. In the  $z < 13.5$  Å range, however, the corrugation character in the two parts of Figure 5 is remarkably different. The tip models in part a) always show anticorrugation at positive bias voltages, and below  $-0.27$  V they provide corrugation characters starting from anticorrugation, then normal corrugation, and again anticorrugation with increasing tip-sample distance. On the other hand, in part b), normal corrugation is found close to the surface, which reverts only once with increasing tip-sample distance in the full studied bias range. These different behaviors can be attributed to the tip orbital characters. It is interesting to notice that none of the considered tip orbitals in part a) are localized in the  $z$ -direction, and they have nodal planes either in the  $yz$  plane ( $p_x$  and  $d_{xz}$ ) or in the  $xz$  plane ( $p_y$  and  $d_{yz}$ ) or in the  $x = y$  and  $x = -y$  planes ( $d_{x^2-y^2}$ ). On the other hand, in part b) there are tips which are localized in the  $z$ -direction ( $p_z$  and  $d_{3z^2-r^2}$ ) or having nodal planes in both the  $xz$  and  $yz$  planes ( $d_{xy}$ ) as well as the spherical  $s$  tip and the W(110) tip that contains all type of orbitals with energy

dependent partial PDOS functions. The particular tip nodal planes restrict the collection of surface atom contributions to specific regions on the sample surface. Furthermore, by changing the tip-sample distance, the orientational overlaps between tip and sample orbitals change, and according to our model some localized orbitals gain more importance in the tunneling contribution, see also Figure 4. Since we calculate the current difference between tip positions above the surface top and hollow sites, the complex tip-sample and bias voltage dependent effect of the real space orbitals on the tunneling can be visualized via the corrugation inversion maps.

Concerning tips with  $p_z$  and  $d_{3z^2-r^2}$  orbital symmetry, Heinze et al. [16] calculated a corrugation enhancement factor of 2 and 6.25, respectively, based on Chen's derivative rule [26]. Moreover, they argued that the corrugation inversion map should be practically identical to the one obtained by using the  $s$ -tip model, and the corrugation values just have to be scaled up by these factors. On the contrary, based on our orbital dependent tunneling model, we find that the  $p_z$  and  $d_{3z^2-r^2}$  tips provide qualitatively different corrugation inversion maps, i.e., although their bias dependent shape is similar to the one of the  $s$ -tip, their tip-sample distance is systematically pushed to larger values, see part b) of Figure 5. This is due to the more localized character of these tip orbitals in the  $z$ -direction.

Corrugation inversion with the  $d_{xy}$  tip occurs at the largest tip-sample distance. A possible explanation can be based on its  $xz$  and  $yz$  nodal planes. While above the top position only the underlying W atom, above the hollow position all four nearest neighbor W atoms give zero contribution to the current, thus,  $I_T$  is expected to be higher than  $I_H$  at small tip-sample distances. To overcome this effect, the tip has to move far from the surface, since then the relative importance of the nearest neighbor contributions decays rapidly compared to other parts of the surface.

For a more realistic W(110) tip, we find that the corrugation inversion map is qualitatively similar to the  $s$ -tip. In the  $[-0.3 \text{ V}, -0.15 \text{ V}]$  bias range they are even almost identical, and the same linear dependence is observed. The similarity of the W(110) tip to the  $s$ -tip has also been found for the current convergence in Figure 3, and it suggests that the common effect of different orbitals of a realistic tip can indeed be close to a spherical tip behavior. However, we stress again that the independent orbital approximation could not reproduce the corrugation inversion effect.

Apart from above findings, we obtain corrugation inversion also in the positive bias range

at enlarged tip-sample distances for the  $s$ ,  $p_z$ ,  $d_{3z^2-r^2}$ , and W(110) tips considered in part b) of Figure 5. This is most probably due to the surface electronic structure and this effect is even more difficult to capture in experiments as the corrugation values themselves decay rapidly with increasing tip-sample distance.

In order to demonstrate the corrugation inversion more apparently, constant current STM images can be simulated. As it is clear from Figure 5, any type of crossing of the  $\Delta I(z, V) = 0$  contour results in the occurrence of the corrugation reversal. In experiments, two ways can be considered to record STM images in the normal and anticorrugated regimes: 1) keep the tip-sample distance  $z$  constant, and change the bias voltage  $V$ , or 2) keep the bias voltage  $V$  constant and change the tip-sample distance. These modes correspond respectively to a horizontal and a vertical crossing of the  $\Delta I(z, V) = 0$  contour in the  $(z, V)$  plane as shown in Figure 5. As the second option seems to be more feasible experimentally, we simulated STM images at a fixed bias voltage of -0.25 V using the W(110) tip, and extracted three different constant current contours. As part b) of Figure 5 shows, at this particular bias voltage a corrugation inversion at  $z = 4 \text{ \AA}$  occurs. Therefore, we chose current values that correspond to current contours with three different apparent heights of the W atom at  $z_T = 3.5 \text{ \AA}$ ,  $4 \text{ \AA}$ , and  $4.5 \text{ \AA}$ . We calculated the tunneling current in a box above the rectangular scan area shown in Figure 2 containing 99000 ( $30 \times 22 \times 150$ ) grid points with a  $0.15 \text{ \AA}$  lateral and  $0.05 \text{ \AA}$  vertical resolution. The constant current contours are extracted following the method described in Ref. [14]. The obtained STM images are shown in Figure 6. In part a)  $\Delta z(I) = z_T(I) - z_H(I) > 0$ , thus, the apparent height of the W atom is larger than the one of the hollow position. The reverse situation is obtained in part c). Part b) corresponds to the situation where the corrugation inversion occurs, i.e.,  $\Delta z(I) = 0$ . In this case we obtain a stripe-like image. This, and all of the simulated STM images are in good agreement with Ref. [16]. We also calculated the corrugation of the individual current contours, and obtained 0.8, 0.3, and 0.2 pm for parts a), b), and c), respectively. These values are extremely small, but are again in good agreement with the reported values in Ref. [16].

Thus, employing our new orbital dependent tunneling model, we could reproduce and reinvestigate the corrugation inversion effect observed on the W(110) surface. Although this effect is driven by the surface electronic structure, we showed that different tips can drastically modify its tip-sample distance and bias voltage dependence.



## IV. CONCLUSIONS

We developed an orbital dependent electron tunneling model and implemented it within the atom superposition approach for simulating STM and STS. Applying our computationally efficient method, we analyzed the convergence and the orbital contributions to the tunneling current above the W(110) surface. We found that the  $d_{3z^2-r^2}-d_{3z^2-r^2}$  contribution is the largest, and depending on the tip position, other  $d$  states can gain importance as well. We also studied the corrugation inversion effect. Using the independent orbital approximation, no corrugation reversal has been obtained at all. Employing the orbital dependent model, we found corrugation reversals depending on the bias voltage and the tip-sample distance, in accordance with the work of Heinze et al. [16]. Explaining this effect, we highlighted the role of the real space shape of the orbitals involved in the tunneling. Moreover, we calculated corrugation inversion maps considering different tip models, and found two qualitatively different behaviors based on the tip orbital symmetry. From these maps, we predicted corrugation reversals for specific tips even at positive bias voltages at enlarged tip-sample distances compared to those at negative bias. Simulation of STM images made the corrugation inversion effect more apparent. Extending this orbital dependent tunneling model to magnetic junctions is expected to enable the study of the interplay of real space orbital and spin polarization effects in SP-STM and SP-STs experiments in the future.

## V. ACKNOWLEDGMENTS

Financial support of the Magyary Foundation, EEA and Norway Grants, the Hungarian Scientific Research Fund (OTKA PD83353, K77771), the Bolyai Research Grant of the Hungarian Academy of Sciences, and the New Széchenyi Plan of Hungary (Project ID: TÁMOP-4.2.2.B-10/1-2010-0009) is gratefully acknowledged. Furthermore, partial usage of the computing facilities of the Wigner Research Centre for Physics is kindly acknowledged.

- 
- [1] M. Bode, Rep. Prog. Phys. **66**, 523 (2003).
  - [2] R. Wiesendanger, Rev. Mod. Phys. **81**, 1495 (2009).
  - [3] W. Wulfhekel and C. L. Gao, J. Phys. Condens. Matter **22**, 084021 (2010).



- [4] W. A. Hofer, A. S. Foster, and A. L. Shluger, *Rev. Mod. Phys.* **75**, 1287 (2003).
- [5] W. A. Hofer, *Prog. Surf. Sci.* **71**, 147 (2003).
- [6] V. A. Ukraintsev, *Phys. Rev. B* **53**, 11176 (1996).
- [7] B. Koslowski, C. Dietrich, A. Tschetschetkin, and P. Ziemann, *Phys. Rev. B* **75**, 035421 (2007).
- [8] M. Passoni, F. Donati, A. Li Bassi, C. S. Casari, and C. E. Bottani, *Phys. Rev. B* **79**, 045404 (2009).
- [9] M. Ziegler, N. Néel, A. Sperl, J. Kröger, and R. Berndt, *Phys. Rev. B* **80**, 125402 (2009).
- [10] B. Koslowski, H. Pfeifer, and P. Ziemann, *Phys. Rev. B* **80**, 165419 (2009).
- [11] T. Kwapinski and M. Jałochowski, *Surf. Sci.* **604**, 1752 (2010).
- [12] K. Palotás, W. A. Hofer, and L. Szunyogh, *Phys. Rev. B* **83**, 214410 (2011).
- [13] W. A. Hofer and A. Garcia-Lekue, *Phys. Rev. B* **71**, 085401 (2005).
- [14] K. Palotás, W. A. Hofer, and L. Szunyogh, *Phys. Rev. B* **84**, 174428 (2011).
- [15] K. Palotás, W. A. Hofer, and L. Szunyogh, *Phys. Rev. B* **85**, 205427 (2012).
- [16] S. Heinze, S. Blügel, R. Pascal, M. Bode, and R. Wiesendanger, *Phys. Rev. B* **58**, 16432 (1998).
- [17] D. Wortmann, S. Heinze, P. Kurz, G. Bihlmayer, and S. Blügel, *Phys. Rev. Lett.* **86**, 4132 (2001).
- [18] H. Yang, A. R. Smith, M. Prikhodko, and W. R. L. Lambrecht, *Phys. Rev. Lett.* **89**, 226101 (2002).
- [19] A. R. Smith, R. Yang, H. Yang, W. R. L. Lambrecht, A. Dick, and J. Neugebauer, *Surf. Sci.* **561**, 154 (2004).
- [20] S. Heinze, *Appl. Phys. A* **85**, 407 (2006).
- [21] M. Passoni and C. E. Bottani, *Phys. Rev. B* **76**, 115404 (2007).
- [22] F. Donati, S. Piccoli, C. E. Bottani, and M. Passoni, *New J. Phys.* **13**, 053058 (2011).
- [23] J. Tersoff and D. R. Hamann, *Phys. Rev. Lett.* **50**, 1998 (1983).
- [24] J. Tersoff and D. R. Hamann, *Phys. Rev. B* **31**, 805 (1985).
- [25] W. Sacks, *Phys. Rev. B* **61**, 7656 (2000).
- [26] C. J. Chen, *Phys. Rev. B* **42**, 8841 (1990).
- [27] P. Ferriani, C. Lazo, and S. Heinze, *Phys. Rev. B* **82**, 054411 (2010).
- [28] M. Bode, M. Heide, K. von Bergmann, P. Ferriani, S. Heinze, G. Bihlmayer, A. Kubetzka,

- O. Pietzsch, S. Blügel, and R. Wiesendanger, *Nature* **447**, 190 (2007).
- [29] S. Heinze, X. Nie, S. Blügel, and M. Weinert, *Chem. Phys. Lett.* **315**, 167 (1999).
- [30] G. Kresse and J. Furthmüller, *Comput. Mater. Sci.* **6**, 15 (1996).
- [31] G. Kresse and J. Furthmüller, *Phys. Rev. B* **54**, 11169 (1996).
- [32] J. Hafner, *J. Comput. Chem.* **29**, 2044 (2008).
- [33] G. Kresse and D. Joubert, *Phys. Rev. B* **59**, 1758 (1999).
- [34] J. P. Perdew and Y. Wang, *Phys. Rev. B* **45**, 13244 (1992).
- [35] H. J. Monkhorst and J. D. Pack, *Phys. Rev. B* **13**, 5188 (1976).

TABLE I: Real space orbitals, their indices used in the present paper, their definition from spherical harmonics  $Y_l^m(\vartheta, \varphi)$ , and the angular dependence of their wave functions  $\chi(\vartheta, \varphi)$ . Note that  $\vartheta$  and  $\varphi$  are the usual polar and azimuthal angles, respectively, in the spherical coordinate system centered on the corresponding (tip or sample) atom.

orbital	index	definition	$\chi(\vartheta, \varphi)$
$s$	1	$Y_0^0$	1
$p_y$	2	$Y_1^1 - Y_1^{-1}$	$\sin(\vartheta)\sin(\varphi)$
$p_z$	3	$Y_1^0$	$\cos(\vartheta)$
$p_x$	4	$Y_1^1 + Y_1^{-1}$	$\sin(\vartheta)\cos(\varphi)$
$d_{xy}$	5	$Y_2^2 - Y_2^{-2}$	$\sin^2(\vartheta)\sin(2\varphi)$
$d_{yz}$	6	$Y_2^1 - Y_2^{-1}$	$\sin(2\vartheta)\sin(\varphi)$
$d_{3z^2-r^2}$	7	$Y_2^0$	$\frac{1}{2}(3\cos^2(\vartheta) - 1)$
$d_{xz}$	8	$Y_2^1 + Y_2^{-1}$	$\sin(2\vartheta)\cos(\varphi)$
$d_{x^2-y^2}$	9	$Y_2^2 + Y_2^{-2}$	$\sin^2(\vartheta)\cos(2\varphi)$

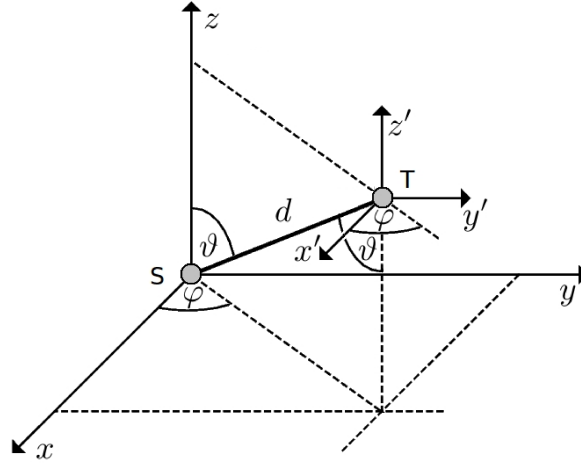


FIG. 1: Geometry of a general tip-sample setup. The  $a$  notation of the surface atom is omitted for brevity.

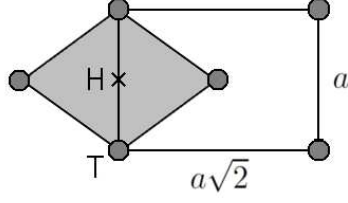


FIG. 2: The surface unit cell of W(110) (shaded area) and the rectangular scan area for the tunneling current simulations. Circles denote the W atoms. The top (T) and hollow (H) positions are explicitly shown.

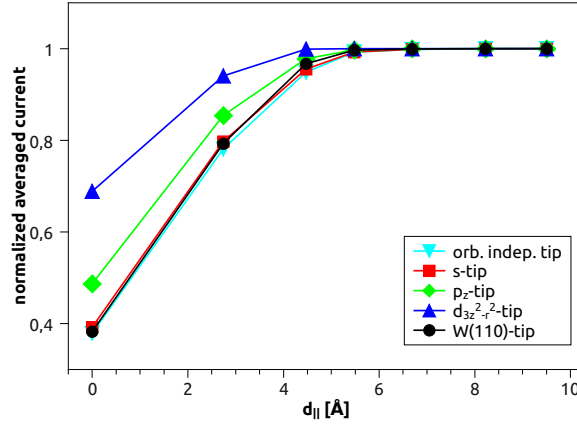


FIG. 3: (Color online) Convergence of the normalized averaged current calculated with different tip models.

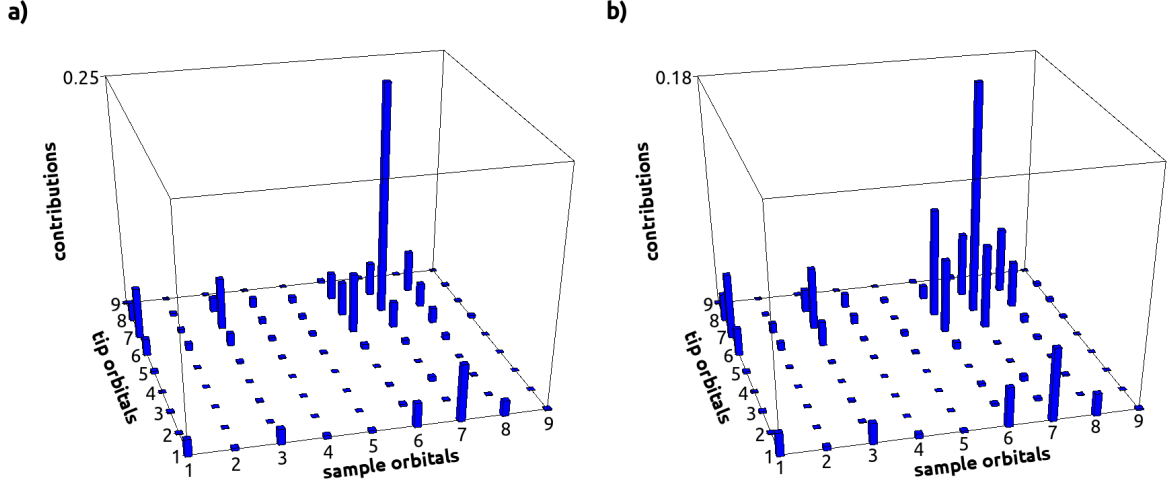


FIG. 4: (Color online) Histograms of the current contributions ( $I_{\beta\gamma}$ ) from all tip-sample transitions with different orbital symmetries using the W(110) tip at  $V = -0.1$  V bias. a) Tip apex  $z = 4.5$  Å above the surface top (T) position (W atom); b) tip apex  $z = 4.5$  Å above the surface hollow (H) position, see also Figure 2. The indices of the atomic orbitals (1-9) follow the notation reported in Table I.

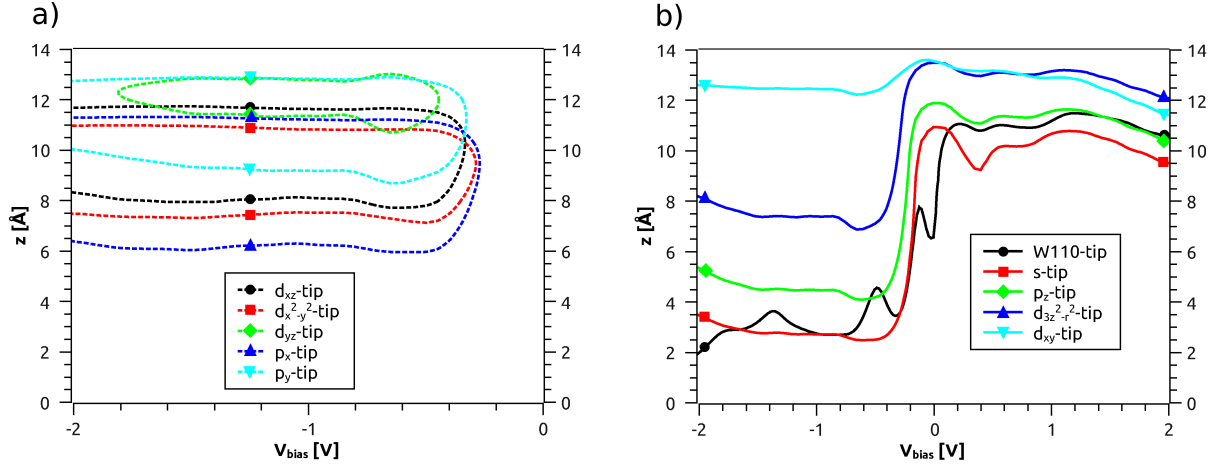


FIG. 5: (Color online) The  $\Delta I(z, V) = I_T(z, V) - I_H(z, V) = 0$  contours indicative for corrugation inversion calculated with different tip models. a) and b) parts show two distinct behaviors depending on the orbital symmetry of the tips. The large tip-sample distance region ( $z > 13.5$  Å) corresponds to  $\Delta I < 0$  in both a) and b) parts.

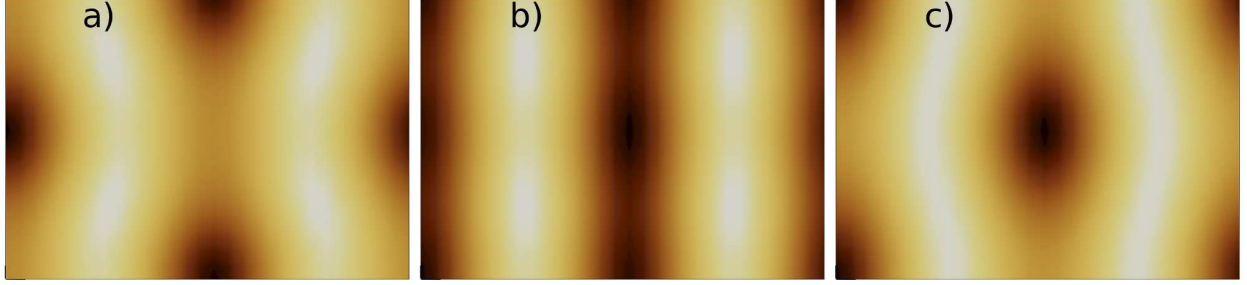


FIG. 6: (Color online) Simulated STM images (constant current contours) at  $V = -0.25$  V bias voltage using the W(110) tip. The scan area corresponds to the rectangle shown in Figure 2. Light and dark areas denote higher and lower apparent heights, respectively. The current values ( $I$ ), the apparent heights of the W atom ( $z_T$ ), and the corrugation of the contours ( $\Delta z'$ ) are as follows: a)  $I = 2.5 \times 10^{-1}$  nA,  $z_T = 3.5$  Å,  $\Delta z' = 0.8$  pm; b)  $I = 9.3 \times 10^{-2}$  nA,  $z_T = 4.0$  Å,  $\Delta z' = 0.3$  pm; c)  $I = 3.4 \times 10^{-2}$  nA,  $z_T = 4.5$  Å,  $\Delta z' = 0.2$  pm.